

# Analyzing Head Orientation of Neurotypical and Autistic Individuals in Triadic Conversations

Onur N. Tepencelik, Wenchuan Wei, Pamela C. Cosman, *Fellow*, IEEE, Sujit Dey, *Fellow*, IEEE

**Abstract**—We propose a system that estimates people’s body and head orientations using low-resolution point cloud data from two LiDAR sensors. Our models make accurate estimations in real-world conversation settings where the subject moves naturally with varying head and body poses. The body orientation estimation model uses ellipse fitting while the head orientation estimation model is a pipeline of geometric feature extraction and an ensemble of neural network regressors. Compared with other body and head orientation estimation systems using RGB cameras, our proposed system uses LiDAR sensors to preserve user privacy, while achieving comparable accuracy. Unlike other body/head orientation estimation systems, our sensors do not require a specified placement in front of the subject. Our models achieve a mean absolute estimation error of 5.2 degrees for body orientation and 13.7 degrees for head orientation. We use our models to quantify behavioral differences between neurotypical and autistic individuals in triadic conversations. Tests of significance show that people with autism spectrum disorder display significantly different behavior compared to neurotypical individuals in terms of distributing attention between participants in a conversation, suggesting that the approach could be a component of a behavioral analysis or coaching system.

**Index Terms**—Autism spectrum disorder, body orientation, head orientation, LiDAR sensor, point cloud, triadic conversation, triadic interaction

## I. INTRODUCTION

Body and head orientation estimation are fundamental challenges in computer vision, mainly investigated in the context of pedestrian protection and movement prediction [1], along with applications in robotics [2] and behavior analysis [3]. Multiple studies [4], [5] have shown that head orientation is a good indicator of visual focus of attention, without the need to estimate gaze orientation. Body and head orientation and movement provide important means of nonverbal communication for fluent social interaction. Individuals with social communication differences (for example, some individuals with Autism Spectrum Disorder (ASD)) might not regularly provide normative nonverbal communication cues, such as periodically making eye contact with a speaker and maintaining a body orientation generally towards them [6]. Differences from society’s workplace communication norms are one reason that high-functioning young adults with ASD have high unemployment rates [7] despite often holding college degrees, average to high IQs, and various useful skills.

This work was supported by the National Science Foundation under grant DUE-1928604.

O.N. Tepencelik, P.C. Cosman and S. Dey are with the Department of Electrical and Computer Engineering, and W. Wei was with the Department of Electrical and Computer Engineering, UC San Diego, La Jolla, CA 92093, USA. (e-mail: {otepence, w8wei, pcosman, dey} @ucsd.edu)

Most work on body and head orientation estimation uses RGB cameras for their low cost and prevalence [3], [8], but more expensive RGB-D cameras such as Microsoft Kinect and Intel RealSense have also been used [9], [10]. However, use of RGB cameras raises privacy concerns in many cases, including our application. Studies suggest that people’s concerns over privacy have been increasing, with privacy protection mechanisms getting more attention [11], [12]. We propose a system that uses point cloud data from LiDAR sensors to estimate body and head orientations while protecting user privacy. While depth maps also preserve privacy, most common depth sensors are RGB-D that record color information as well, whereas LiDAR solely outputs depth, making it a more privacy-safe device [13]. There has been increased adoption of LiDAR sensors with declining costs [14], [15]. Many recent projects in different fields such as healthcare [13], [16], security, and surveillance [17], [18], have adopted LiDAR sensors over privacy invading alternatives. With recent advances in LiDAR technology and big data management systems that enable data scalability [19], they are likely to become more prevalent in stores, workplaces, and hospitals.

Available depth image-based models using RGB-D sensors or LiDAR seemed to be good candidates for our need to estimate body and head orientation during conversations. However, these models require the sensor to be placed in front of the person, with specific optimal ranges for distance and height, which we refer to as a *frontal setting*. In contrast, our system does not require the subject to appear head-on in front of the sensor. Our sensors are placed near the ceiling, looking down at about 45 degrees, and the subject can have arbitrary orientation in the conference area; we refer to this as a *surveillance setting*. Our models for body and head orientation estimation with LiDAR sensors are the first that permit a surveillance viewpoint. In general, surveillance settings produce low resolution data; a subject farther from the sensor is represented with fewer points in a point cloud or fewer pixels in an RGB image. Especially for head pose estimation, most models [20], [21] use high-resolution 3D scans of the head, taken by a sensor close to the subject. With such a setting, it is possible to capture small facial geometric details of the nose tip, eye holes, and chin, which can play a huge role for orientation estimation. While those models are successful for high-resolution data, they face challenges in our case, as our sensors are unobtrusively distant from the people, and it is difficult to identify small facial geometry features due to the decreasing resolution and increasing noise with distance.

To analyze behaviors related to body and head orientation, we use a triadic conversation setting with two *interviewers*

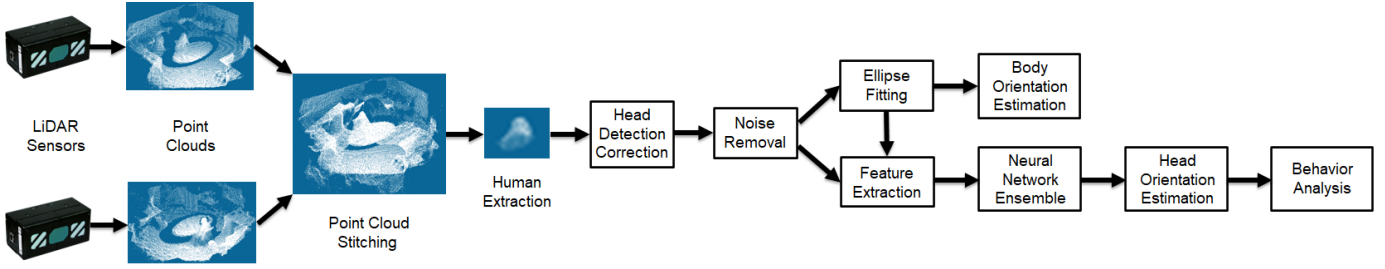


Fig. 1. System overview.

and one *subject* sitting around an oval conference table. Triadic conversations are common in professional and social settings. Adjusting body and head orientation in such settings is important to engage with both of the other people and make everyone feel included in the conversation [22]. In triadic interactions, some individuals with ASD tend to fixate on one person while ignoring the other for some time [23], a non-normative distribution of attention which could be seen as non-inclusive or socially inappropriate. Other common neurodivergent behaviors include not making eye contact with any of the interviewers while speaking, or not paying attention to a speaker while listening [24], [25]. Our body and head orientation estimation system can quantify such behavioral differences between neurodivergent and neurotypical individuals. We plan to extend our system to provide coaching and feedback to autistic individuals, imitating the coaching advice of a professional behavioral coach, with the motivation of supporting autistic individuals in practicing conversational engagement skills in preparation for job interviews and workplace communications [26], [27].

Our contributions in this paper include the development of body and head orientation estimation models based on low resolution point cloud data, generated by two indoor LiDAR sensors from a surveillance viewpoint. Fig. 1 shows the system overview. A preliminary version of this work [26] estimated head yaw angle using a limited set of body and head poses involving a motionless subject with a straight body, lowered arms, and a head pose with no roll or pitch rotations. The current work, enhancing the model in [26], is able to estimate orientations while the subject moves naturally and displays various body and head poses. The enhanced model can estimate yaw with similar accuracy even in the presence of roll and pitch rotations. Our second main contribution is quantifying differences in orienting behavior between neurotypical and neurodivergent individuals using an automated system. Although some of these differences are generally known to characterize ASD, we are the first to quantify them using an automated system, and the first to quantify them in a triadic conversation setting.

## II. RELATED WORK

Body and head orientation estimation are well studied tasks in computer vision. In this section, we categorize related work according to the data types (RGB images or depth maps/point clouds) as well as the experiment setting (frontal or surveillance). We then introduce a few studies that analyze

and compare orienting behaviors of neurotypical and autistic individuals in similar experimental settings.

### A. Body Orientation Estimation

Among the many RGB image-based models for body orientation estimation which are generally in the context of smart vehicles and robotics for human-robot interactions, there are a few which match our type of surveillance setting. Chen *et al.* [3] proposed a semi-supervised model on RGB images to analyze behavior and attention based on estimated body and head orientations of people waiting for luggage in an airport. The authors of [28] and [29] proposed template matching models that combine 2D images from multiple surveillance viewpoints to make 3D orientation estimates. Studies targeting pedestrian orientation [30]–[33] usually approach the problem as a classification task, providing less precision compared to regression models. Many studies such as [34], [35] incorporated motion information and tracking techniques into their models as they approach the task from the perspective of a vehicle. The authors of [8], [36] proposed models to estimate body orientation for human-robot interactions, which resemble a frontal setting.

The few works on body orientation estimation using depth sensors do not use surveillance scenarios. Shimizu *et al.* [37] proposed a model which combines shape and motion information using a LiDAR-mounted robot. Similarly, [38] combines Histogram of Oriented Gradient (HOG) features with motion information tracked by a Kalman filter, using depth images from a Kinect sensor. Other studies use depth along with color information; [39] enhanced features extracted from an RGB image using depth and motion information, while [40] combined features extracted from both RGB and depth images. Experimenting with different CNN architectures that use RGB input, depth input and RGB-D input, authors of [2] argued that depth maps are more suitable for estimating orientation than RGB images.

### B. Head Orientation Estimation

Many papers estimate all three Euler angles (yaw, pitch, roll) to define a full head pose [9], [10]. Depending on the application, such as behavior prediction on pedestrians [3], [33], pitch and roll angles are often neglected as yaw angle defines the direction people are looking. For our application on the division of attention between two other people in a triadic conversation, we likewise focus on yaw angle.

As with body orientation, the majority of models in the literature use RGB images, but some use depth, and only a

few consider the task in a surveillance setting. Before deep learning techniques, good results were achieved by [41]–[43] using graph embedding, manifold learning and locally linear embedding techniques. Zhao *et al.* [44] used a neural network followed by more complex architectures such as random regression forests [45], deep neural networks [46], [47], convolutional neural networks (CNN) [48]–[51] and Graph-CNNs [52]. All these papers target a frontal setting. The authors of [3], [53] created various models and surveillance settings for the head orientation estimation task using RGB cameras, as the latter took advantage of extensive research on face detection in a room surveyed by four cameras creating multi-view representations. The authors of [1] proposed RGB image based head orientation estimation models, to ensure pedestrian safety from the perspective of a vehicle. Similarly, a CNN-based model in [33] estimated pedestrian orientations from a surveillance viewpoint. While proposing a transfer learning approach, the authors of [54] published the DPOSE dataset, a dynamic, multi-view head pose dataset collected in a room with 4 cameras at surveillance viewpoints. Various papers [55], [56] proposed new methods and published results on the DPOSE dataset. A CNN-based model in [57] works on unconstrained RGB images, similar to a surveillance viewpoint with higher resolution.

Head orientation estimation using depth cameras has a longer history (see [58]) compared to body orientation estimation using depth cameras. Following the availability of consumer-level depth cameras such as Microsoft Kinect and Intel RealSense, various head orientation estimation models using depth images [9], [10], [20], [21], [59]–[61] were proposed. The BIWI benchmark [9] contains around 15000 samples of head poses recorded with a sensor placed frontally about 1 meter from the subjects, and it was used for many results [10], [20], [21], [52], [55], [62]. A particle swarm optimization approach was used in [21], while [20] used triangular surface patches as hand-crafted 3D features to estimate orientation. More recent papers such as [10], [62] proposed CNN architectures to tackle the problem; [62] resembles our work as their model uses 3D point clouds as input as opposed to the more common 2D depth maps. Point clouds were also used in [63] which leveraged the PointNet++ architecture [64] by using its abstraction layers as a feature extractor, and they further improved their work by including temporal information using an LSTM network in [65]. Similar to the depth information based body orientation estimation models, the models listed above assume that the depth sensor is directly in front of the person.

To our knowledge, we are the first to estimate body and head orientations using a depth sensor from a surveillance viewpoint. Existing models use either RGB images with a surveillance setting, or use depth images with a frontal setting.

### C. Analysis of Orientation Behavior

As suggested by [66], early triadic behaviors are important for the development of later social responsiveness. The authors of [23] studied triadic conversations with low communicative intent (researchers speaking primarily with each other, with occasional input from a child) and dyadic conversations with

high communicative intent (a researcher directly interacting with a child) and found that children with ASD made 57% more gaze fixations to people’s faces in these triadic conversations compared to the dyadic ones; the reverse pattern was found for typically developing (TD) children. The authors also found that children with ASD spent 12.3% less time looking at other people’s faces in these triadic conversations compared to the dyadic ones, and 9.7% less compared to TD children.

Other studies such as [67], [68] with different experimental settings also provide insight into orienting behaviors of people with ASD. The authors of [67] found that children with autism were significantly less likely to respond to social stimuli (such as calling the child’s name, or snapping fingers) with a re-orientation of the head, compared to their responses to non-social stimuli (such as a phone ringing), as well as compared to the responses of TD children. In a virtual public speaking experiment, the authors of [68] found that high-functioning children with ASD made contact with the listeners less frequently compared to TD children.

Many researchers have studied social modulation of gaze, which is the change in gaze orientation based on conversational role (e.g., speaker or listener). In dyadic conversations, listeners generally gaze more at speakers compared to speakers looking at listeners [69]–[71]. However, [71] found that in group conversations, the gaze levels of speakers come close to that of listeners. The authors argued that one reason for this change was that speakers, when addressing a group, need to collect visual feedback from each individual and to maintain the signal that they are addressing each individual.

## III. DATA SETS

Our system uses two ToFv2 LiDAR sensors from Hitachi Vantara [72]. The sensors capture depth information and create a point cloud based on the Time-of-Flight principle [73]. We placed sensors at opposite ceiling corners in a 3x3.5 meter conference room, looking down on an oval table. The point clouds are stitched together using rotation and translation. We use the sensor software’s built-in human detector which outputs XY-coordinates of the center of gravity of the detected human, as well as a Z-coordinate of the top of the head,  $Z_{head}$ . This study was approved by the UC San Diego Institutional Review Board (Protocol 210775, Date 7/1/2021).

### A. Static Dataset

In [26], we created a static dataset from 15 subjects with and without glasses and face masks, and with varying hairstyles and heights. We collected data with one subject at a time, while the subject follows guidance arrows (as ground truth) placed on a table. Each subject orients their head towards 13 predetermined angles (-90 to +90 degrees, in increments of 15 degrees). For capturing each point cloud, the subjects are instructed to be motionless with their upper body straight to the front and parallel to the table edge, and with their hands on the table or on their lap.

### B. Conversation Dataset

To create a dataset that represents natural aspects of a conversation, we recorded conversations in a triangular conversational setting with two interviewers and one subject. The

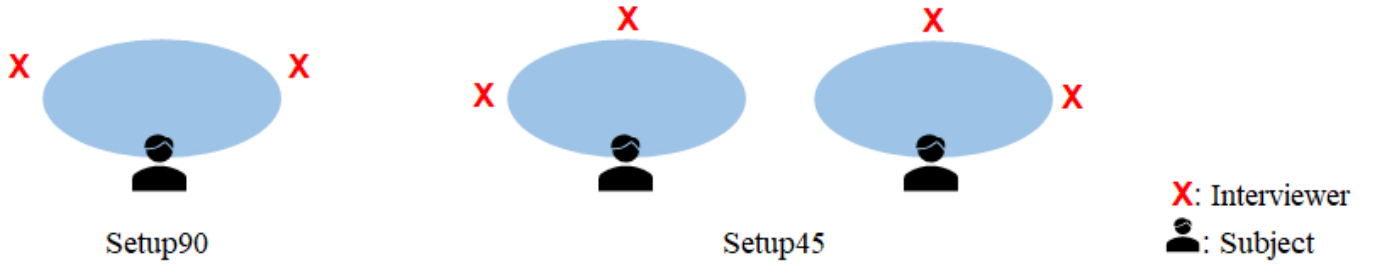


Fig. 2. Conversation Setups

subjects were 12 neurodivergent individuals who had received a community diagnosis of ASD and 8 neurotypical individuals. Each subject participated in 2 sessions of 8 to 15 minutes where the interviewers changed seating positions between the sessions to capture different head and body orientations from the subjects. The subjects were asked to engage naturally as they would in a casual conversation, and they were not informed prior to the session that the data would be used to analyze head and body orientation. During the sessions, LiDAR point cloud data were recorded with an average frame rate of 1.5 fps. We also recorded RGB video solely for ground truth labeling and not for model development. Unlike the static dataset, in the conversational setting we observed many different body poses by the subjects, such as turning their upper body towards one interviewer, using their arms and hands as part of their body language, and putting their hands close to their face while thinking or listening.

To create a dataset that contains various head poses that occur during a real conversation, we manually sampled and labeled data from the sessions. To manually estimate the ground truth head orientation from video snapshots, we used 3 reference orientations. Two of these are computed using the point cloud centroid coordinates of the two interviewers with respect to the subject, at the time of the snapshot. The third reference angle is the average of the first two, representing the midpoint of the two interviewers. For example, if one interviewer is seated 30 degrees to the left of the subject, and the other interviewer is seated 50 degrees to the right, the three reference angles are +30, -50 and -10 degrees. If the subject’s head is oriented directly towards an interviewer, the ground truth label is the reference angle for that interviewer. If the subject is looking at the midpoint of the two interviewers (a common situation when speaking to multiple listeners), the ground truth label is the midpoint reference angle. We collected data in two different experimental setups, as shown in Fig. 2. In *Setup90*, the interviewers are separated by an angle of around 90 degrees (ranging from 75 to 105 across sessions) from the subject’s perspective, whereas in *Setup45*, the separation is around 45 degrees (ranging between 35 and 55 degrees). Different seating positions helped us sample and label data with different head orientations, creating useful variety in the dataset. The manual sampling and labeling procedure is detailed below:

- 1) Align the RGB video and point cloud recordings based on timestamps.

- 2) From the video recording, identify an instance where the subject’s head orientation is static for at least two seconds and close to a reference point.
- 3) Extract the point cloud data that corresponds to the identified video instance.
- 4) Calculate the reference angles using the point cloud coordinates of the subject and the interviewers.
- 5) Estimate the subject’s head orientation from the video as ground truth, with the help of reference angles.

From this, we obtained 80 to 140 instances from each ASD subject, totaling 1400 point cloud frames. It is important to note that this process is done only once to establish ground truth for creating the model, and should not be construed as a calibration step needed in subsequent use of the model.

This manual sampling and labeling is subject to potential human errors. Estimating head orientation accurately from a video is hard, although we sampled instances where the subject’s head is oriented towards an interviewer or the midpoint, which are relatively easier positions to interpret the orientation. To quantify the human labeling error, we conducted a simple experiment on three subjects. Using guidance arrows to guide the subject to adjust their head orientation in 5 degree increments, we collected a random sequence of head orientations. On average, human labels based on video recordings differed by about 4.5 degrees from the guidance arrow ground truth. A portion of this error comes from the subjects imperfectly aligning their heads with the guidance arrows, which is a potential issue that exists in the static dataset as well.

### C. Data Cleaning

Our dataset presented challenges in data cleaning. First, there were issues caused by the sensors. Network overload during real-time data collection caused lost point cloud frames that were replaced by previously recorded frames, an issue present in 3 of 24 data collection sessions. Of the 1400 point clouds manually sampled from the real-time sessions, 56 were excluded as they were sampled from a repetition sequence and therefore did not reflect the true state of the environment at the matched timestamp. Another LiDAR sensor issue was the inaccuracy of the built-in human detection algorithm. The sensor may confuse the subject’s shoulder with their head, resulting in a wrong output of center of gravity and  $Z_{head}$ . In that case, the wrong portion of the human body is cropped out and the point cloud lacks points from the other shoulder. We removed an additional 74 point clouds due to this erroneous

human detection. In Section IV-B, our proposed head position estimation algorithm can mitigate this issue.

Secondly, there are human errors during manual sampling and labeling, such as selecting a wrong timestamp from the video recording, or a slight lack of synchronization between the video recording and point cloud sequence, leading to the selection of the wrong point cloud frame. In such instances, we observed that the next or previous point cloud is more suitable for the suggested head orientation label, indicating that the wrong point cloud was sampled and the subject’s head orientation changed within consecutive frames. We address this problem by using our model’s predictions on the neighboring frames as a preliminary indication of a wrong sampling or a synchronization issue, and replace the point cloud with its neighbor if we can visually confirm the issue from the video recording and point cloud sequence. In Fig. 3, two consecutive point clouds from one of our data sequences are shown. The human labeler originally sampled Fig. 3a from the sequence, trying to match with the video instance where the subject’s head was towards an interviewer seated 35 degrees to the subject’s left. However, due to a slight synchronization issue, the point cloud in Figure 3a belongs to the middle of the head movement towards that interviewer, and the next point cloud (shown in Figure 3b) should have been sampled instead. The head movement becomes apparent when 4-5 consecutive point clouds are visualized on top of each other and compared with the corresponding video sequence, which allows one to choose the point cloud matching the intended orientation label. Of the remaining 1270 point clouds, 41 were replaced by their neighboring point clouds due to this labeling issue.

## IV. METHODOLOGY

### A. Pre-Processing

For this work, we introduced additional pre-processing steps compared to our work in [26]. As explained in Section IV-B, the built-in head height estimation is often inaccurate, so we propose an improved estimation procedure to obtain the head height,  $Z_{head}$ . To extract the region of interest which consists of the upper body and head, we crop a cylinder-shaped boundary around each person’s point cloud using the centroid and a radius of 50 cm. For each subject, a threshold for the upper body set empirically as the top 27% of their height (in a seated position) is computed from our improved estimated  $Z_{head}$ . We also removed points from the head point cloud if they are at least 15 cm away from the head center and from the upper body point cloud if they are at least 25 cm away from the body center on the horizontal plane, after separating the head and upper body point clouds. The computation of head and body centroids and the separation of head and upper body point clouds are explained in Section IV. With these additional steps, we were able to remove points that did not belong to the region of interest and instead belong to the table, the back of the chair, or noise, which created many distortions in our preliminary work [26].

The upper body point clouds obtained from the pre-processing step consist of about 1800 points on average, varying between about 1500 and 2100 points per case. Since our system is in a surveillance setting, our upper body point

clouds are low resolution compared to other work, e.g., the BIWI dataset [9] contains around 10,000 points for a person’s face alone. Estimating body and head orientation from low-resolution LiDAR data is challenging due to the lack of detail in the small region of interest. Moreover, the point cloud data from the surveillance angle are noisy, especially from hair and other complex features on the head. To mitigate this, we apply a k-nearest neighbor noise removal step, where we delete a point if the average distance between the point and its 10 nearest neighbors is larger than 50 mm.

### B. Head Position Correction

Although the LiDAR’s built-in human detection capability usefully extracts human point clouds from the environment point cloud, it does not pinpoint the head center in the horizontal plane as the center of gravity of the human is not necessarily the same as their head center. The algorithm also provides inconsistent results for  $Z_{head}$ . The two sensors make independent estimates which are averaged to form a joint estimate, which is usually better than relying on a single sensor estimate. However if one sensor makes a large estimation error, the joint estimation is not good enough to recover. Accurate and consistent estimation of  $Z_{head}$  across the whole dataset is especially important as it is used to separate the head and upper body point clouds.

We improved the estimate of the head center and  $Z_{head}$  from the point cloud. If  $Z_1$  and  $Z_2$  (in centimeters) represent the built-in  $Z_{head}$  estimates for sensors 1 and 2, we use  $Z = ((Z_1 + Z_2)/2) - 15$  as the initial separation threshold; points above this threshold belong to the head and points below belong to the upper body. This yields two disjoint point clouds,  $PC_{head}$  and  $PC_{body}$ . We project the points in  $PC_{head}$  onto the horizontal plane and use least-squares ellipse fitting on them, as detailed in the following section. The ellipse center is a more accurate estimate of the head center, compared to the built-in estimate from the LiDAR sensors.  $Z_{head}$  is determined by sorting the points by their z-coordinate and taking the highest point with a maximum height difference of 1mm with the next 5 highest points. This operation mitigates noise distorting the  $Z_{head}$  calculation, and generally pinpoints the top of the head where the height difference between points should be saturated. The head center computed from the least-squares ellipse, together with this  $Z_{head}$ , represent the center point of the subject’s top of the head.

This improves our preliminary work [26], which relied heavily on the built-in estimates. In [26], the inaccurate built-in estimation for  $Z_{head}$  was used to base the separation threshold to obtain  $PC_{head}$  and  $PC_{body}$ , which sometimes caused  $PC_{head}$  to contain points from the shoulders or  $PC_{body}$  to contain points from the chin.

### C. Body Orientation Estimation

The body orientation estimation model is a geometric model which takes advantage of the ability to change the viewpoint from which a point cloud is seen, and uses the birds-eye view of the room. The cropped point clouds are projected onto the horizontal plane. After estimating  $Z_{head}$ , we separate head and body points using a refined threshold of  $Z = Z_{head} - 17.5$

and calculate the 2D ellipse that best fits the projected  $PC_{body}$  based on least squares error, with the long axis of the ellipse representing the frontal (shoulder-to-shoulder) axis. We use the conic representation of an ellipse:

$$E(x, y) = ax^2 + bxy + cy^2 + dx + ey + f = 0 \quad (1)$$

The optimal coefficients are estimated as in [74]. The noise removal pre-processing is important for this procedure to work well, as noise points that are generally on the edges may result in large squared errors. The correction of the built-in  $Z_{head}$  estimation is also crucial as explained in the previous section.

After the frontal axis is determined, there remains the issue of which side of the ellipse is the front. We calculate the average perpendicular distance of each point in  $PC_{head}$  from both sides to the frontal axis. Assuming that a person’s head is almost always in front of their body (their frontal axis), the front is taken as the side with higher average perpendicular distance. In our datasets, this assumption holds true 99.7% of the time and the front side is correctly determined.

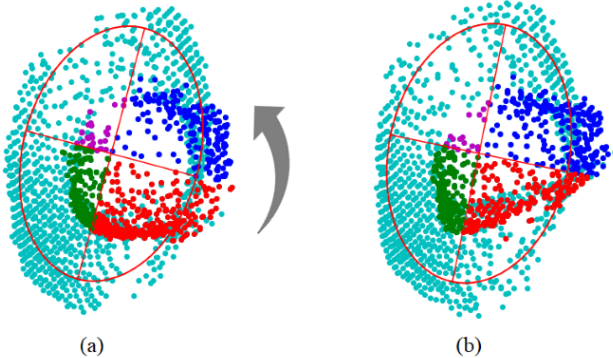


Fig. 3. Least squares ellipse fitting for body orientation estimation via the long axis of the fitted ellipse, which also determines the four quadrants of the head relative to the body. Light blue points are projected upper body points (shoulders and chest); dark blue, red, purple and green points are projected head points, representing the four quadrants, in order. The first and second quadrants represent the front-left and front-right sides of the head, respectively; while the third and fourth quadrants represent the back-left and back-right sides of the head. (a) Head orientation label unknown; point cloud belongs to a head movement that starts at 0 degrees and moves to the left (b) Head orientation labeled as 35 degrees to the left.

#### D. Feature Extraction and Selection

For head orientation estimation, simple geometric approaches were not sufficient as details of facial features are not accurately captured by the sensors. Therefore, we engineered our own geometric features from the point clouds. The surveillance setting allows low-level geometric features but, given the low resolution of our data, higher level 3D features such as surface patches [9], [20] or curvatures [75]–[77] did not produce useful results on our dataset. The approach proposed in [63], using the initial layers of PointNet++ to extract feature representations, or a Graph-CNN approach proposed in [62] similarly did not suit our data. However, as shown in our prior work [26] and the current study, our low-level geometric features allow estimation of head orientation with reasonable accuracy in a low resolution surveillance setting.

The feature extraction is done after noise removal and ellipse fitting to the upper body. The upper body ellipse divides  $PC_{head}$  into four quadrants which produce supportive features

for the model, based on the point locations with respect to the body center. Fig. 3 shows two projected human point clouds, the optimal ellipse fit for body orientation estimation, and the resulting four quadrants of the head for each of the clouds.

The features we extract are the  $(x, y)$  coordinates of the subject’s centroid in the sensor coordinate system, as well as a number of features that use a subject-centric coordinate system. These features are the principal components and the basic distribution properties of the points in  $PC_{head}$  (mean, standard deviation, minimum and maximum coordinates), as well as of the points in its four quadrants separately, the estimated nose coordinates based on the centroid of the 10 furthest projected points from the head center, and the axis lengths and orientations of a separate ellipse fitting procedure on  $PC_{head}$ . These features extracted from a single point cloud constitute a feature vector with 103 entries (as x and y dimensions produce distinct features).

For a low resolution regression task, a feature space with over 100 dimensions presents a higher likelihood of overfitting. To mitigate this, we use the Random Forest Recursive Feature Elimination (RF-RFE) process [78], [79] which involves repeatedly training a random forest regressor, ranking the features according to their importance, and eliminating the least important feature(s) in each iteration. This approach has been successfully used in many studies [80]–[82]. After applying RF-RFE, the optimal feature set had 42-dimensions, with principal components proving to be important features along with some engineered features such as the estimated nose position and the head ellipse parameters.

#### E. Head Orientation Estimation

For head orientation estimation, we use a pipeline of feature extraction and an ensemble of multi-layer perceptron-based regression networks. To train the head orientation estimation model, we use leave-one-out cross-validation, where the point clouds of each subject are used one time as the test set, and used in training otherwise. Thus each neurodivergent subject has their own model that has never seen that subject before, and for neurotypical subjects, we use a model trained with the whole dataset of samples from neurodivergent subjects.

Neural networks are typically high variance estimators, as was our preliminary model [26]. A dataset of noisy low resolution point clouds leads to even more variance in predictions. To reduce the estimation variance and improve overall model performance [83]–[85], we enhanced our initial model by deploying an ensemble of neural networks, where each individual network was initialized with different random weights. Often, different initial weights are enough to generate significantly different models [84]–[86], to create a diverse ensemble. To create the ensemble, we train 20 separate models and rank them based on their performance on the validation set. Then we use Forward Subset Selection [84], [87] to select the models as follows. We start with an initial ensemble of 3 best models, and iteratively add the next best model in the pool to the ensemble until the ensemble performance on the validation set does not improve with the addition of a new model. We ended up with ensembles that contain 3 to 8 models, with the mode and median being 6 models.

TABLE I  
MAE IMPROVEMENT FOR HEAD ORIENTATION ESTIMATION AFTER EACH DATA CLEANING AND PROCESSING STEP

| Process  | Mean Absolute Error on Conversation Dataset |                                   |
|--|---|-----------------------------------|
|  | Model Trained with Conversation Dataset     | Model Trained with Static Dataset |
| Initial Model (from [26] but trained as specified in column) | 19.6  | 35.1                              |
| Head position correction (Sec. IV-A)                         | 18.3  | 32.8                              |
| Removing repeated point clouds (Sec. III-C)                  | 17.2  | 32.8                              |
| Removing point clouds with missing points (Sec. III-C)       | 15.9  | 29.5                              |
| Using neural network ensembles (Sec. IV-E)                   | 14.2  | 26.4                              |
| Fixing wrongly synchronized point clouds (Sec. III-C)        | 13.7  | 26.4                              |

## V. RESULTS

### A. Error Metrics

We primarily use mean absolute error (MAE) to evaluate model performance. For the body orientation estimation model applied to the static dataset, with our proposed improvements, we achieve an MAE of 5.21 degrees compared to the MAE of 8.37 degrees reported in [26]. The model improved significantly with the head position correction presented in Section IV-B.

We train and evaluate the head orientation estimation model on data sampled from our new conversation dataset, from 12 autistic subjects. We use a different model for each subject, where data from the other 11 subjects are used for training. On average, our new modeling approach produces an MAE of 13.73 degrees across 12 leave-one-out models for head orientation estimation. When the model from [26] that was trained with only the static dataset is applied to the 12 subjects on the conversation dataset, the MAE is 26.4 degrees due to the challenges caused by different body poses and natural movements in real-world settings. Our new model based on our conversation dataset outperforms our model in [26] by about 50% in a conversational setting. In [26], we reported an MAE of 12.69 on our experimental static setting, showing that our new model is able to reach similar levels of accuracy in a conversational setting. A more detailed summary is presented in Table I which shows the development of our final model as well as a comparison with our initial model.

Fig. 4 shows the evolution of model performance (MAE) as we eliminate features with the RF-RFE procedure described in Section IV-D. Without RF-RFE, using the whole feature space, the model performance would have been 13% worse compared to the optimal feature set, with an MAE of 15.72 degrees. The MAE of the model with only 1 feature is 25.61 degrees, 46% worse than the optimal model performance.

After obtaining the optimal feature set using the RF-RFE procedure, we conducted some experiments to analyze feature importance. Fig. 5 compares model performance in terms of MAE with the optimal feature set and its subsets in which certain features are excluded. The figure shows the importance of engineered features, including the estimated nose position, principal components of the head quadrants, and parameters of the head ellipse.

While some papers achieve smaller errors on head orientation estimation, they use either high-resolution 3D scans of the face when the sensor is placed directly in front of the person [9], [10], [20], [21], [59]–[61], or an RGB camera [45]–[48]. But for those studies which used indoor RGB

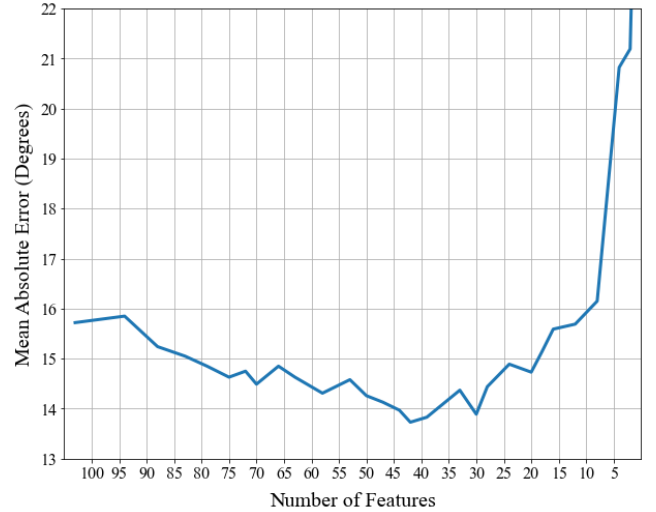


Fig. 4. Evolution of mean absolute estimation error with the Random Forest Recursive Feature Elimination procedure. The initial MAE with 103 features is 15.72 degrees, whereas the MAE with only 1 feature left in the feature space is 25.61 degrees. The optimal feature set contains 42 features and leads to an MAE of 13.73 degrees.

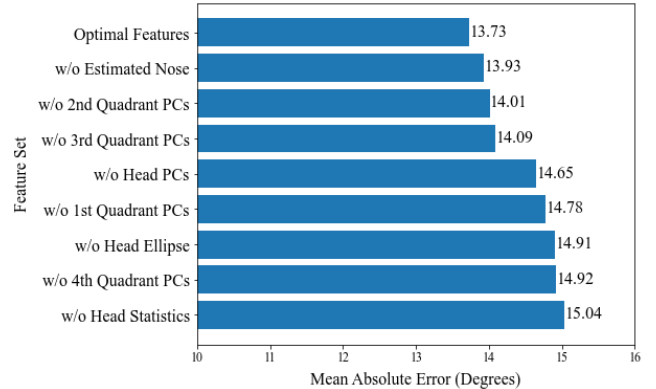


Fig. 5. Performance of optimal feature set and its subsets (PC = Principal Component).

surveillance datasets, MAE values of 19, 23.6, 31 and 33.6 degrees were reported [1], [3], [55] and [53], respectively. While we outperform the above studies which used RGB cameras from surveillance viewpoints in terms of raw MAE numbers, it is hard to make exact comparisons as the datasets are not unified and each dataset has its own challenges. Many studies approach the head orientation estimation problem as a classification task. Authors of [33] report a classification accuracy above 90% where the orientation classes are the 8 main directions, separated by 45 degrees. While such classification might be adequate for applications like pedestrian safety, our behavior analysis application requires more precise estimates.

TABLE II  
COMPARISON OF NEUROTYPICAL AND AUTISTIC SUBJECTS ON TWO EXPERIMENTAL SETUPS

| Statistic  | Setup90 |       | Setup45 |       |
|--|---------|-------|---------|-------|
|  | ASD     | NT    | ASD     | NT    |
| Average duration of contact                        | 11.8    | 6.3   | 7.7     | 6.1   |
| Maximum duration of contact                        | 48.8    | 16.5  | 24.6    | 16.5  |
| Average duration of NOT contacting anyone          | 53.2    | 41.1  | 58.6    | 30.9  |
| Number of contacts per minute                      | 0.84    | 1.37  | 1.44    | 2.15  |
| Total duration of contact % during an interview    | 11.5%   | 13.4% | 15.6%   | 16.6% |
| Maximum duration of exclusions                     | 50.3    | 16.4  | 20.3    | 9.3   |
| Number of exclusions per minute                    | 0.28    | 0.10  | 0.19    | 0.11  |
| Total duration of exclusions % during an interview | 15.5%   | 4.2%  | 7.4%    | 3.1%  |

### B. Behavior Analysis of Neurodivergent and Neurotypical Individuals

In this section, we quantify some orienting behaviors of neurodivergent and neurotypical individuals in two experimental triadic conversation setups, as shown in Fig. 2.

To quantify behaviors, we define the following two terms: *Contact* and *Exclusion*. Based on studies that suggest “2 to 3 seconds” [88], [89] or “a few seconds” [90] of eye contact is optimal when addressing multiple people to connect and make them feel included in the conversation, *Contact* in our context is defined as 3 consecutive frames where the head orientation is inside the region of an interviewer, where a frame is about 0.7 seconds and an interviewer’s region is defined as  $\pm 15^\circ$  from their position. Making occasional contact with an interviewer is important to make them feel included in the conversation [91] and maintain the signal that they are being addressed [71]. *Exclusion* is defined over a 20-frame window; if there are at least 15 estimated head orientations in the region of one interviewer and none in the region of the other, the other interviewer is considered to be excluded from the conversation. In Table II, we present statistics related to *Contact* and *Exclusion* extracted from our conversation sessions using our head orientation estimation model. We present the averages for each statistic across 12 sessions with neurodivergent subjects and across 8 sessions with neurotypical subjects in each setup.

From Table II, we observe that the orienting behaviors of the autistic and neurotypical individuals diverge more in *Setup90*, compared to *Setup45*. When the interviewers are further apart, the autistic individuals have more difficulty with distributing their attention between two conversational partners. Neurotypical subjects tend to make contact with the interviewers in shorter bursts, whereas autistic individuals frequently dwell on one interviewer for a longer period of time. With shorter and more frequent contacts, neurotypical individuals are more likely to ensure that both interviewers feel included in the conversation. Autistic individuals more often have an exclusion, seen through the much higher maximum exclusion duration and total percentage of time spent while an interviewer is excluded.

The authors of [68] suggested that children with ASD made fewer contacts with listeners while speaking to multiple people, compared to typically developing children. Our findings are consistent with this, as we observe from Table II that

TABLE III  
DISTRIBUTION OF HEAD ORIENTATIONS WHILE SUBJECT IS LISTENING

| Head Orientation - Listening | Setup90 |       | Setup45 |       |
|------------------------------|---------|-------|---------|-------|
|                              | ASD     | NT    | ASD     | NT    |
| Interviewer who is speaking  | 27.1%   | 29.2% | 27.4%   | 28.4% |
| Neutral                      | 67.6%   | 67.4% | 65.5%   | 65.6% |
| Other interviewer            | 4.9%    | 3.7%  | 5.5%    | 4.9%  |

TABLE IV  
DISTRIBUTION OF HEAD ORIENTATIONS WHILE SUBJECT IS SPEAKING

| Head Orientation - Speaking | Setup90 |       | Setup45 |       |
|-----------------------------|---------|-------|---------|-------|
|                             | ASD     | NT    | ASD     | NT    |
| Interviewer who spoke last  | 30.3%   | 22.2% | 22.1%   | 18.9% |
| Neutral                     | 55.2%   | 60.8% | 63.0%   | 64.7% |
| Other interviewer           | 14.1%   | 17.1% | 13.4%   | 15.3% |

people with ASD made fewer contacts per minute and spent less total time in contact with the listeners.

We examined statistical significance with independent sample t-tests on the data of the two groups. In *Setup90*, we found that the maximum duration of exclusions and total duration of exclusions percentage during an interview exhibit significantly different results between the two groups,  $t(18) = 2.53, p = 0.014$  and  $t(18) = 2.69, p = 0.011$ , respectively. No significant difference was observed for the *Exclusion* statistics in *Setup45*, supporting the idea that distributing attention was harder in *Setup90* compared to *Setup45* for the ASD participants. Among *Contact* statistics, the average duration of not making contact with anyone was significantly higher in *Setup90* for autistic individuals in comparison with neurotypical individuals,  $t(18) = 1.84, p = 0.046$ . The number of contacts per minute was significantly lower for people with ASD, in both *Setup90* and *Setup45*,  $t(18) = -2.21, p = 0.023$  and  $t(18) = -1.95, p = 0.037$ , respectively.

In Tables III and IV, we present the distributions of head orientations based on the role of the subject in the conversation. In this analysis, we again observe that the differences between the two groups are more evident in *Setup90*. The table shows that, when speaking to multiple people, autistic individuals tend to distribute their attention less evenly; their focus usually remains on the person who made the last remark. Neurotypical individuals pay slightly more attention on the



person who spoke last, while generally ensuring that the other interviewer is also included in the conversation. This difference is confirmed to be significant by t-tests, as the results reveal that people with ASD tend to look at the interviewer who spoke last significantly more than neurotypical people do,  $t(18) = 1.87, p = 0.038$ . To the best of our knowledge, this is the first quantification of these types of differences about conversational roles and their impact on orienting in triadic settings.

Overall, we conclude that there are noticeable differences between the two groups, and our model is able to reflect and quantify these differences. This is important for our eventual goal of creating a coaching tool which would allow autistic individuals to undertake situational practice. While there are many studies regarding social communication behaviors of autistic people, none of them address these in the context of three-way conversations among adults. Quantifying such differences between the groups using an automated system is one of our contributions. Using behavioral studies of individuals with ASD such as [24], [25], one can make educated guesses on attention and orienting behaviors of high-functioning adults with ASD in triadic conversations. As far as we know, we are the first to conduct experiments that validate such guesses and share statistics comparing neurotypical and neurodivergent individuals in triadic conversational settings.

## VI. CONCLUSION

In this paper, we improve our proposed models in [26] for body and head orientation estimation that work with low resolution point clouds generated by two LiDAR sensors. We improve the average error rate of our body orientation estimation model from 8.4 degrees to 5.2 degrees. We enhance our head orientation estimation model by enabling reliable estimations in realistic scenarios where the subject is naturally moving with various head and body poses in a triadic conversation setting. Our estimation results are comparable to results in the literature, although our models work with low-resolution and noisy point clouds and without color information.

One of the future goals of this work is to create a privacy-preserving system that could be used as a virtual coach to allow situational practice of body and head poses during conversations or meetings. Towards this goal, we created a surveillance scenario with LiDAR sensors placed near the ceiling of a conference room and developed novel models that are capable of distinguishing between neurotypical and neurodivergent individuals based on their head and body orientation behavior. We provide novel analysis on various behaviors in triadic interaction settings and show the differences between autistic and neurotypical individuals using statistical significance tests.

In future iterations of this work, we can improve data collection; the network overload issue can be prevented by using a sensor that supports a 1 Gbps network instead of 100 Mbps, as well as a more powerful CPU. The estimated head positions from the built-in human detection algorithm will be corrected using our head detection algorithm presented in Section IV-B.

The proposed body and head orientation estimation models can be used in various applications. We plan to extend our models to become a component of virtual coaching to high-functioning autistic individuals who are seeking jobs, to integrate them to workplaces. To achieve this, we will develop automated smart coaches that leverage the differences between neurotypical and neurodivergent individuals, while imitating the decisions of a professional behavioral coach. When developing a virtual behavioral coaching system, a main consideration is whether and how to provide real-time nudges towards normative behaviors. While the computational power is available to make estimates and provide guidance in real-time with this model, the system could also be used as a non-real-time social behavior analysis tool for autistic people by providing feedback based on their overall display of attentiveness and non-verbal communication in a meeting. Other considerations include the medium (smart watch notifications, vibrations, audio etc.) and the content of the alerts or feedback.

## ACKNOWLEDGMENTS

We thank Ara Jung, Trent Simmons, Sarah Luo and Saygin Artiran for helping with data collection, Sarah Hacker and Ara Jung for managing the IRB approval and subject payments, and all the participants in our study.

## REFERENCES

- [1] E. Rehder, H. Kloeden, and C. Stiller, "Head detection and orientation estimation for pedestrian safety," in *17th Intl. IEEE Conf. on Intelligent Transportation Systems (ITSC)*. IEEE, 2014, pp. 2292–2297.
- [2] B. Lewandowski, D. Seichter, T. Wengefeld, L. Pfennig, H. Drumm, and H.-M. Gross, "Deep orientation: Fast and robust upper body orientation estimation for mobile robotic applications," in *IROS*, 2019, pp. 441–448.
- [3] C. Chen and J.-M. Odobez, "We are not contortionists: Coupled adaptive learning for head and body orientation estimation in surveillance video," in *2012 IEEE Conf. on Computer Vision and Pattern Recognition*. IEEE, 2012, pp. 1544–1551.
- [4] S. O. Ba and J.-M. Odobez, "A study on visual focus of attention recognition from head pose in a meeting room," in *Intl. Workshop on Machine Learning for Multimodal Interaction*. Springer, 2006, pp. 75–87.
- [5] R. Stiefelhagen, J. Yang, and A. Waibel, "Estimating focus of attention based on gaze and sound," in *Proc. of the 2001 Workshop on Perceptive User Interfaces*, 2001, pp. 1–9.
- [6] V. H. Bal, S.-H. Kim, M. Fok, and C. Lord, "Autism spectrum disorder symptoms from ages 2 to 19 years: Implications for diagnosing adolescents and young adults," *Autism Research*, vol. 12, no. 1, pp. 89–99, 2019.
- [7] J. L. Chen, G. Leader, C. Sung, and M. Leahy, "Trends in employment for individuals with autism spectrum disorder: A review of the research literature," *Review Journal of Autism and Developmental Disorders*, vol. 2, no. 2, pp. 115–127, 2015.
- [8] Y. Kohari, J. Miura, and S. Oishi, "CNN-based human body orientation estimation for robotic attendant," in *IAS-15 Workshop on Robot Perception of Humans*, 2018.
- [9] G. Fanelli, T. Weise, J. Gall, and L. Van Gool, "Real time head pose estimation from consumer depth cameras," in *Joint Pattern Recognition Symposium*. Springer, 2011, pp. 101–110.
- [10] G. Borghi, M. Fabbri, R. Vezzani, S. Calderara, and R. Cucchiara, "Face-from-depth for head pose estimation on depth images," *IEEE Trans. on Pattern Analysis and Machine Intelligence*, vol. 42, no. 3, pp. 596–609, 2018.
- [11] L. Stark, A. Stanhaus, and D. L. Anthony, "'I don't want someone to watch me while I'm working': Gendered views of facial recognition technology in workplace surveillance," *Journal of the Association for Information Science and Technology*, vol. 71, no. 9, pp. 1074–1088, 2020.

- [12] D. P. Bhawe, L. H. Teo, and R. S. Dalal, "Privacy at work: A review and a research agenda for a contested terrain," *Journal of Management*, vol. 46, no. 1, pp. 127–164, 2020.
- [13] J.-E. Joo, Y. Hu, S. Kim, H. Kim, S. Park, J.-H. Kim, Y. Kim, and S.-M. Park, "An indoor-monitoring LiDAR sensor for patients with alzheimer disease residing in long-term care facilities," *Sensors*, vol. 22, no. 20, p. 7934, 2022.
- [14] "Lidar market: Forecast and analysis 2022-2028: Skyquest." [Online]. Available: <https://skyquestt.com/report/lidar-market>
- [15] "Follow the latest trend news in the semiconductor industry," Apr 2022. [Online]. Available: <https://www.yolegroup.com/product/report/lidar--market--technology-trends-2022/>
- [16] M. Bouazizi, C. Ye, and T. Ohtsuki, "Activity detection using 2D LIDAR for healthcare and monitoring," in *2021 IEEE Global Communications Conf. (GLOBECOM)*. IEEE, 2021, pp. 01–06.
- [17] A. Günter, S. Böker, M. König, and M. Hoffmann, "Privacy-preserving people detection enabled by solid state LiDAR," in *2020 16th Intl. Conf. on Intelligent Environments (IE)*. IEEE, 2020, pp. 1–4.
- [18] B. Rodrigues, L. Müller, E. J. Scheid, M. F. Franco, C. Killer, and B. Stiller, "LaFlector: a privacy-preserving LiDAR-based approach for accurate indoor tracking," in *2021 IEEE 46th Conf. on Local Computer Networks (LCN)*. IEEE, 2021, pp. 367–370.
- [19] C. N. Lokugam Hewage, D. F. Laefer, A.-V. Vo, N.-A. Le-Khac, and M. Bertolotto, "Scalability and performance of LiDAR point cloud data management systems: A state-of-the-art review," *Remote Sensing*, vol. 14, no. 20, p. 5277, 2022.
- [20] C. Papazov, T. K. Marks, and M. Jones, "Real-time 3D head pose and facial landmark estimation from depth images using triangular surface patch features," in *Proc. of the IEEE Conf. on Computer Vision and Pattern Recognition*, 2015, pp. 4722–4730.
- [21] P. Padeleris, X. Zabulis, and A. A. Argyros, "Head pose estimation on depth data based on particle swarm optimization," in *2012 IEEE Computer Society Conf. on Computer Vision and Pattern Recognition Workshops*. IEEE, 2012, pp. 42–49.
- [22] A. Nagels, T. Kircher, M. Steines, and B. Straube, "Feeling addressed! the role of body orientation and co-speech gesture in social communication," *Human Brain Mapping*, vol. 36, no. 5, pp. 1925–1936, 2015.
- [23] A. McParland, S. Gallagher, and M. Keenan, "Investigating gaze behaviour of children diagnosed with autism spectrum disorders in a classroom setting," *Journal of Autism and Developmental Disorders*, vol. 51, no. 12, pp. 4663–4678, 2021.
- [24] D. American Psychiatric Association, A. P. Association et al., *Diagnostic and Statistical Manual of Mental Disorders: DSM-5*. American Psychiatric Association Washington, DC, 2013, vol. 5.
- [25] W. H. Organization et al., *The ICD-10 Classification of Mental and Behavioural Disorders: Clinical Descriptions and Diagnostic Guidelines*. World Health Organization, 1992.
- [26] O. N. Tepencelik, W. Wei, L. Chukoskie, P. C. Cosman, and S. Dey, "Body and head orientation estimation with privacy preserving LiDAR sensors," in *2021 29th European Signal Processing Conf. (EUSIPCO)*. IEEE, 2021, pp. 766–770.
- [27] S. Artiran, L. Chukoskie, A. Jung, I. Miller, and P. Cosman, "HMM-based detection of head nods to evaluate conversational engagement from head motion data," in *2021 29th European Signal Processing Conf. (EUSIPCO)*. IEEE, 2021, pp. 1301–1305.
- [28] L. Chen, G. Panin, and A. Knoll, "Human body orientation estimation in multiview scenarios," in *Intl. Symposium on Visual Computing*. Springer, 2012, pp. 499–508.
- [29] M. C. Liem and D. M. Gavrilu, "Person appearance modeling and orientation estimation using spherical harmonics," in *2013 10th IEEE Intl. Conf. and Workshops on Automatic Face and Gesture Recognition (FG)*. IEEE, 2013, pp. 1–6.
- [30] M.ENZWEILER and D. M. Gavrilu, "Integrated pedestrian classification and orientation estimation," in *2010 IEEE Computer Society Conf. on Computer Vision and Pattern Recognition*. IEEE, 2010, pp. 982–989.
- [31] J. Tao and R. Klette, "Part-based RDF for direction classification of pedestrians, and a benchmark," in *Asian Conf. on Computer Vision*. Springer, 2014, pp. 418–432.
- [32] H. Liu and L. Ma, "Online person orientation estimation based on classifier update," in *2015 IEEE Intl. Conf. on Image Processing (ICIP)*. IEEE, 2015, pp. 1568–1572.
- [33] M. Raza, Z. Chen, S.-U. Rehman, P. Wang, and P. Bao, "Appearance based pedestrians' head pose and body orientation estimation using deep learning," *Neurocomputing*, vol. 272, pp. 647–659, 2018.
- [34] F. Flohr, M. Dumitru-Guzu, J. F. Kooij, and D. M. Gavrilu, "A probabilistic framework for joint pedestrian head and body orientation estimation," *IEEE Trans. on Intelligent Transportation Systems*, vol. 16, no. 4, pp. 1872–1882, 2015.
- [35] I. Ardiyanto and J. Miura, "Partial least squares-based human upper body orientation estimation with combined detection and tracking," *Image and Vision Computing*, vol. 32, no. 11, pp. 904–915, 2014.
- [36] C. Weinrich, C. Vollmer, and H.-M. Gross, "Estimation of human upper body orientation for mobile robotics using an SVM decision tree on monocular images," in *2012 IEEE/RSJ Intl. Conf. on Intelligent Robots and Systems*. IEEE, 2012, pp. 2147–2152.
- [37] M. Shimizu, K. Koide, I. Ardiyanto, J. Miura, and S. Oishi, "LIDAR-based body orientation estimation by integrating shape and motion information," in *2016 IEEE Intl. Conf. on Robotics and Biomimetics (ROBIO)*. IEEE, 2016, pp. 1948–1953.
- [38] B. S. B. Dewantara, R. W. A. Saputra, and D. Pramadihanto, "Estimating human body orientation from image depth data and its implementation," *Machine Vision and Applications*, vol. 33, no. 3, pp. 1–19, 2022.
- [39] W. Liu, Y. Zhang, S. Tang, J. Tang, R. Hong, and J. Li, "Accurate estimation of human body orientation from RGB-D sensors," *IEEE Trans. on Cybernetics*, vol. 43, no. 5, pp. 1442–1452, 2013.
- [40] T. Ji, L. Liu, W. Zhu, J. Wei, and S. Wei, "Fast and efficient integration of human upper-body detection and orientation estimation in RGB-D video," in *2017 IEEE 9th Intl. Conf. on Communication Software and Networks (ICCSN)*. IEEE, 2017, pp. 1178–1181.
- [41] Y. Fu and T. S. Huang, "Graph embedded analysis for head pose estimation," in *7th Intl. Conf. on Automatic Face and Gesture Recognition (FG06)*. IEEE, 2006, pp. 6–pp.
- [42] B. Raytchev, I. Yoda, and K. Sakaue, "Head pose estimation by nonlinear manifold learning," in *Proc. of the 17th Intl. Conf. on Pattern Recognition, 2004. ICPR 2004.*, vol. 4. IEEE, 2004, pp. 462–466.
- [43] V. N. Balasubramanian, J. Ye, and S. Panchanathan, "Biased manifold embedding: A framework for person-independent head pose estimation," in *2007 IEEE Conf. on Computer Vision and Pattern Recognition*. IEEE, 2007, pp. 1–7.
- [44] L. Zhao, G. Pingali, and I. Carlbom, "Real-time head orientation estimation using neural networks," in *Proc. Intl. Conf. on Image Processing*, vol. 1. IEEE, 2002, pp. 1–1.
- [45] G. Fanelli, J. Gall, and L. Van Gool, "Real time head pose estimation with random regression forests," in *CVPR 2011*. IEEE, 2011, pp. 617–624.
- [46] B. Ahn, J. Park, and I. S. Kweon, "Real-time head orientation from a monocular camera using deep neural network," in *Asian Conf. on Computer Vision*. Springer, 2014, pp. 82–96.
- [47] B. Ahn, D.-G. Choi, J. Park, and I. S. Kweon, "Real-time head pose estimation using multi-task deep neural network," *Robotics and Autonomous Systems*, vol. 103, pp. 1–12, 2018.
- [48] H.-W. Hsu, T.-Y. Wu, S. Wan, W. H. Wong, and C.-Y. Lee, "Quatnet: Quaternion-based head pose estimation with multiregression loss," *IEEE Trans. on Multimedia*, vol. 21, no. 4, pp. 1035–1046, 2018.
- [49] Z. Hu, Y. Xing, C. Lv, P. Hang, and J. Liu, "Deep convolutional neural network-based Bernoulli heatmap for head pose estimation," *Neurocomputing*, vol. 436, pp. 198–209, 2021.
- [50] H. Liu, H. Nie, Z. Zhang, and Y.-F. Li, "Anisotropic angle distribution learning for head pose estimation and attention understanding in human-computer interaction," *Neurocomputing*, vol. 433, pp. 310–322, 2021.
- [51] H. Liu, T. Liu, Z. Zhang, A. K. Sangaiah, B. Yang, and Y. Li, "ARHPE: asymmetric relation-aware representation learning for head pose estimation in industrial human-computer interaction," *IEEE Trans. on Industrial Informatics*, vol. 18, no. 10, pp. 7107–7117, 2022.
- [52] M. Xin, S. Mo, and Y. Lin, "EVA-GCN: Head pose estimation based on graph convolutional networks," in *Proc. of the IEEE/CVF Conf. on Computer Vision and Pattern Recognition*, 2021, pp. 1462–1471.
- [53] Z. Zhang, Y. Hu, M. Liu, and T. Huang, "Head pose estimation in seminar room using multi view face detectors," in *Intl. Evaluation Workshop on Classification of Events, Activities and Relationships*. Springer, 2006, pp. 299–304.
- [54] A. K. Rajagopal, R. Subramanian, R. L. Vieriu, E. Ricci, O. Lanz, K. Ramakrishnan, and N. Sebe, "An adaptation framework for head-pose classification in dynamic multi-view scenarios," in *Asian Conf. on Computer Vision*. Springer, 2012, pp. 652–666.
- [55] C. Hong, J. Yu, J. Zhang, X. Jin, and K.-H. Lee, "Multimodal face-pose estimation with multitask manifold deep learning," *IEEE Trans. on Industrial Informatics*, vol. 15, no. 7, pp. 3952–3961, 2018.
- [56] Y. Yan, E. Ricci, R. Subramanian, O. Lanz, and N. Sebe, "No matter where you are: Flexible graph-guided multi-task learning for multi-view head pose classification under target motion," in *Proc. of the IEEE Intl. Conf. on Computer Vision (ICCV)*, December 2013.

- [57] R. Berral-Soler, F. J. Madrid-Cuevas, R. Muñoz-Salinas, and M. J. Marín-Jiménez, "RealHePoNet: a robust single-stage convnet for head pose estimation in the wild," *Neural Computing and Applications*, vol. 33, no. 13, pp. 7673–7689, 2021.
- [58] S. Malassiotis and M. G. Strintzis, "Robust real-time 3D head pose estimation from range data," *Pattern Recognition*, vol. 38, no. 8, pp. 1153–1165, 2005.
- [59] F. A. Kondori, S. Yousefi, H. Li, S. Sonning, and S. Sonning, "3D head pose estimation using the Kinect," in *2011 Intl. Conf. on Wireless Communications and Signal Processing (WCSP)*. IEEE, 2011, pp. 1–4.
- [60] R. S. Ghiass, O. Arandjelović, and D. Laurendeau, "Highly accurate and fully automatic head pose estimation from a low quality consumer-level RGB-D sensor," in *Proc. of the 2nd Workshop on Computational Models of Social Interactions: Human-Computer-Media Communication*, 2015, pp. 25–34.
- [61] M. Martin, F. Van De Camp, and R. Stiefelhagen, "Real time head model creation and head pose estimation on consumer depth cameras," in *2014 2nd Intl. Conf. on 3D Vision*, vol. 1. IEEE, 2014, pp. 641–648.
- [62] Y. Xu, C. Jung, and Y. Chang, "Head pose estimation using deep neural networks and 3D point clouds," *Pattern Recognition*, vol. 121, p. 108210, 2022.
- [63] T. Hu, S. Jha, and C. Busso, "Robust driver head pose estimation in naturalistic conditions from point-cloud data," in *2020 IEEE Intelligent Vehicles Symposium (IV)*. IEEE, 2020, pp. 1176–1182.
- [64] C. R. Qi, L. Yi, H. Su, and L. J. Guibas, "PointNet++: Deep hierarchical feature learning on point sets in a metric space," *Advances in Neural Information Processing Systems*, vol. 30, 2017.
- [65] T. Hu, S. Jha, and C. Busso, "Temporal head pose estimation from point cloud in naturalistic driving conditions," *IEEE Trans. on Intelligent Transportation Systems*, 2021.
- [66] S. Clifford and C. Dissanayake, "Dyadic and triadic behaviours in infancy as precursors to later social responsiveness in young children with autistic disorder," *Journal of Autism and Developmental Disorders*, vol. 39, no. 10, pp. 1369–1380, 2009.
- [67] G. Dawson, K. Toth, R. Abbott, J. Osterling, J. Munson, A. Estes, and J. Liaw, "Early social attention impairments in autism: social orienting, joint attention, and attention to distress." *Developmental Psychology*, vol. 40, no. 2, p. 271, 2004.
- [68] W. Jarrold, P. Mundy, M. Gwaltney, J. Bailenson, N. Hatt, N. McIntyre, K. Kim, M. Solomon, S. Novotny, and L. Swain, "Social attention in a virtual public speaking task in higher functioning children with autism," *Autism Research*, vol. 6, no. 5, pp. 393–410, 2013.
- [69] A. Kendon, "Some functions of gaze-direction in social interaction," *Acta Psychologica*, vol. 26, pp. 22–63, 1967.
- [70] M. Argyle and M. Cook, "Gaze and mutual gaze." 1976.
- [71] R. Vertegaal, R. Slagter, G. Van der Veer, and A. Nijholt, "Eye gaze patterns in conversations: there is more to conversational agents than meets the eyes," in *Proc. of the SIGCHI Conf. on Human Factors in Computing Systems*, 2001, pp. 301–308.
- [72] "Hitachi Vantara 3D LiDAR," <https://www.hitachivantara.com/en-us/products/video-intelligence/devices/3d-lidar-sensor.html>, [Online].
- [73] R. Lange and P. Seitz, "Solid-state time-of-flight range camera," *IEEE Journal of Quantum Electronics*, vol. 37, no. 3, pp. 390–397, 2001.
- [74] F. L. Bookstein, "Fitting conic sections to scattered data," *Computer Graphics and Image Processing*, vol. 9, no. 1, pp. 56–71, 1979.
- [75] M. P. P. Segundo, L. Silva, O. R. P. Bellon, and C. C. Queirolo, "Automatic face segmentation and facial landmark detection in range images," *IEEE Trans. on Systems, Man, and Cybernetics, Part B (Cybernetics)*, vol. 40, no. 5, pp. 1319–1330, 2010.
- [76] Y. Sun and L. Yin, "Automatic pose estimation of 3D facial models," in *2008 19th Intl. Conf. on Pattern Recognition*. IEEE, 2008, pp. 1–4.
- [77] K. I. Chang, K. W. Bowyer, and P. J. Flynn, "Multiple nose region matching for 3D face recognition under varying facial expression," *IEEE Trans. on Pattern Analysis and Machine Intelligence*, vol. 28, no. 10, pp. 1695–1700, 2006.
- [78] I. Guyon, J. Weston, S. Barnhill, and V. Vapnik, "Gene selection for cancer classification using support vector machines," *Machine Learning*, vol. 46, no. 1, pp. 389–422, 2002.
- [79] P. M. Granitto, C. Furlanello, F. Biasioli, and F. Gasperi, "Recursive feature elimination with random forest for ptr-ms analysis of agroindustrial products," *Chemometrics and Intelligent Laboratory Systems*, vol. 83, no. 2, pp. 83–90, 2006.
- [80] P. Misra and A. S. Yadav, "Improving the classification accuracy using recursive feature elimination with cross-validation," *Intl. Journal of Emerging Technologies*, vol. 11, no. 3, pp. 659–665, 2020.
- [81] K. Zvarevashe and O. O. Olugbara, "Gender voice recognition using random forest recursive feature elimination with gradient boosting machines," in *2018 Intl. Conf. on Advances in Big Data, Computing and Data Communication Systems (ICABCD)*. IEEE, 2018, pp. 1–6.
- [82] S. Ustebay, Z. Turgut, and M. A. Aydin, "Intrusion detection system with recursive feature elimination by using random forest and deep learning classifier," in *2018 Intl. Congress on Big Data, Deep Learning and Fighting Cyber Terrorism (IBIGDELFT)*. IEEE, 2018, pp. 71–76.
- [83] L. K. Hansen and P. Salamon, "Neural network ensembles," *IEEE Trans. on Pattern Analysis and Machine Intelligence*, vol. 12, no. 10, pp. 993–1001, 1990.
- [84] J. Mendes-Moreira, C. Soares, A. M. Jorge, and J. F. D. Sousa, "Ensemble approaches for regression: A survey," *ACM Computing Surveys (CSUR)*, vol. 45, no. 1, pp. 1–40, 2012.
- [85] Y. Ren, L. Zhang, and P. N. Suganthan, "Ensemble classification and regression-recent developments, applications and future directions," *IEEE Computational Intelligence Magazine*, vol. 11, no. 1, pp. 41–53, 2016.
- [86] J. Kolen and J. Pollack, "Back propagation is sensitive to initial conditions," *Advances in Neural Information Processing Systems*, vol. 3, 1990.
- [87] M. P. Perrone and L. N. Cooper, "When networks disagree: Ensemble methods for hybrid neural networks," Brown Univ. Providence RI Inst. for Brain and Neural Systems, Tech. Rep., 1992.
- [88] S. Weinschenk, *100 Things Every Presenter Needs to Know About People*. New Riders, 2012.
- [89] W. Steele, *Presentation Skills 201: How to Take It to the Next Level as a Confident, Engaging Presenter*. Outskirts Press, 2009. [Online]. Available: <https://books.google.com/books?id=PYJmPgAACAAJ>
- [90] R. Ailes, *You Are the Message: Getting What You Want by Being Who You Are*. Currency, 2012.
- [91] R. Vertegaal and Y. Ding, "Explaining effects of eye gaze on mediated group conversations: amount or synchronization?" in *Proc. of the 2002 ACM Conf. on Computer Supported Cooperative Work*, 2002, pp. 41–48.